ORGANOMETALLICS

Article

pubs.acs.org/Organometallics

Unsaturated Triosmium Carbonyl Cluster Complexes with Bridging Aryl Ligands: Structures, Bonding, and Transformations

Richard D. Adams,* Vitaly Rassolov,* and Qiang Zhang

Department of Chemistry and Biochemistry, University of South Carolina, Columbia, South Carolina 29208, United States

Supporting Information

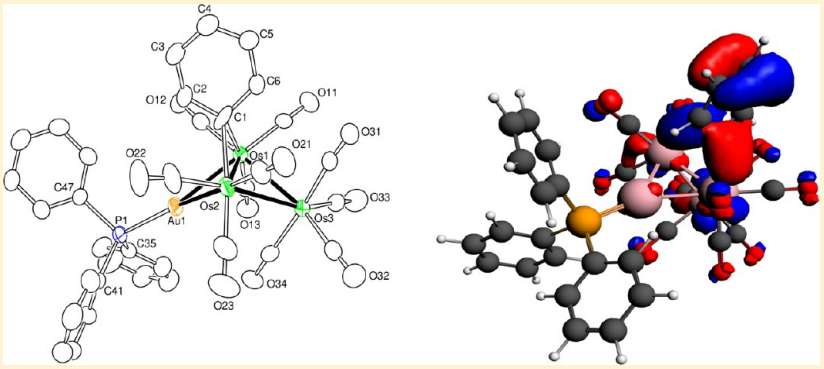

ABSTRACT: Reactions of $Os_3(CO)_{10}(NCMe)_2$, **1**, with the series of aryl-gold complexes $ArylAu(PPh_3)$ [Aryl = phenyl = Ph, 2-naphthyl = 2-Np (2-$C_{10}H_7$) and 1-pyryl (1-$C_{16}H_{10}$)] have provided the series of electronically unsaturated triosmium complexes $Os_3(CO)_{10}(\mu$-η^1-Ar)(μ-$AuPPh_3$) [**2**, Ar = phenyl = Ph; **3**, Ar = 2-naphthyl = 2-Np (2-$C_{10}H_7$); and Ar = **4** and **5**, 2-pyryl and 4-pyryl], containing bridging η^1-Ar ligands and a bridging $Au(PPh_3)$ group that bridges the same unsaturated Os−Os bond in the 46-electron cluster complex. All new compounds were characterized by single-crystal X-ray diffraction analyses. A DFT computational analysis of **2** has revealed that bonding of the bridging phenyl ligand to the metal atoms consists of a combination of delocalized σ-bonding between the ipso-carbon atom and the two proximate metal atoms and π-donation from the π-orbitals of the ring to those same metal atoms. There is no significant metal to ring π-back-bonding. Compound **3** exists as two isomers, **3a** and **3b**. Compound **3a** contains a μ-η^1-2-Np ligand. Compound **3b** contains a μ-η^2-2-Np ligand. The pyryl complexes **4** and **5** also exist as two isomers. These differ by the point of attachment of the η^1-Ar ligand to the metal atoms. When heated to reflux in an octane solution (125 °C), compounds **2**, **3**, **4**, and **5** were decarbonylated and converted to the corresponding aryne complexes $Os_3(CO)_9(\mu_3$-Ar)(μ-$AuPPh_3$)(μ-H), **6**−**9**, which contain a triply bridging aryne ligand formed by the loss of one CO ligand from the complex and by a CH cleavage on the bridging Ar ligand. A mechanism for the transformation of **3b** into the naphthyne complex **7** was established by DFT computational analyses.

INTRODUCTION

Metal complexes containing aryl ligands are of great interest as intermediates for a variety of important catalytic reactions, especially cross-couplings,[1] direct arylations,[2] and hydroarylations.[3] Aryl ligands in copper-based complexes generally adopt bridging coordination modes.[4] There are a number of reports of bridging aryl ligands among the polynuclear transition metal carbonyl complexes.[5] In most cases, η^1-bridging aryl ligands bridge two similar metal atoms in a symmetrical fashion, **A**.[4,5] η^1-Aryl ligands bridging heteronuclear pairs of metal atoms are often coordinated asymmetrically, **B**.[4a,6,7] We have chosen to describe these asymmetrical η^1-bridging aryl ligands as *semibridging* ligands.[7] η^1-Bridging aryl ligands serve as one-electron donors. There are also a few reported examples of η^2-bridging aryl ligands **C**. These ligands are generally regarded as three-electron donors.[8]

The activation of CH bonds in aromatic compounds is of great interest.[2,3] Johnson and Lewis showed that the triosmium carbonyl complex $Os_3(CO)_{10}(NCMe)_2$, **1**, reacts with arenes by cleavage of two adjacent CH bonds to yield the complexes $Os_3(CO)_{10}(\mu_3$-$C_6H_2R^1R^2)(\mu$-$H)_2$ (R^1, R^2 = H, H; H, Me; H, Pr^n; H, CHCHPh; H, Cl; Me, Me), which contain a triply bridging aryne ligand.[9] There is considerable interest in the coordination and reactivity of aryne ligands in polynuclear metal complexes.[10] Very little has been done to establish the mechanism(s) of the CH activation step(s) in the formation of these aryne compounds. Johnson et al. did show that the triply bridging η^6-C_6H_6 ligand in the complex $Os_3(CO)_9(\mu_3$-$C_6H_6)$ could be

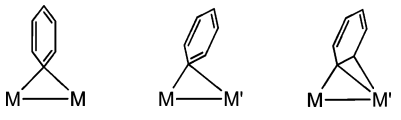

A B C

Received: July 25, 2013
Published: October 11, 2013

converted into a benzyne ligand in the complex $Os_3(CO)_9(\mu_3\text{-}C_6H_4)(\mu\text{-}H)_2$ under the influence of UV−vis irradiation.[11]

The electronic similarities between H and the $Au(PPh_3)$ group are well known.[12] We have recently initiated studies of the reactions of $C_6H_5Au(PPh_3)$ with polynuclear metal carbonyl complexes in the hopes of learning more about the nature of CH activation processes as they might relate to those in C_6H_6.[13,14] In this work, we have prepared the first examples of electronically unsaturated triosmium carbonyl complexes that contain η^1-bridging aryl ligands via reactions of **1** with a series of aryl-gold complexes $ArylAu(PPh_3)$ [Aryl = phenyl = Ph, 1-naphthyl = 1-Np ($1\text{-}C_{10}H_7$) and 1-pyryl ($1\text{-}C_{16}H_{10}$)]. Unsaturated metal carbonyl cluster complexes are of interest because they exhibit higher reactivity than their electronically saturated counterparts.[15] We have recently shown that these bridging aryl ligands undergo hindered rotation about the metal−metal bond.[16] The bridging aryl groups in these complexes can be converted into triply bridging aryne ligands by thermal decarbonylations that involve CH activations on the aryl ring systems. A preliminary report of this work has been published.[14]

EXPERIMENTAL DETAILS

General Data. Reagent grade solvents were dried by the standard procedures and were freshly distilled prior to use. Infrared spectra were recorded on a Thermo Nicolet Avatar 360 FT-IR spectrophotometer. Room-temperature ^1H NMR and $^{31}P\{^1H\}$ NMR spectra were recorded on a Bruker Avance/DRX 400 NMR spectrometer operating at 400.3 and 162.0 MHz, respectively. Positive/negative ion mass spectra were recorded on a Micromass Q-TOF instrument by using electrospray (ES) ionization. UV−vis absorption spectra were recorded on a JASCO Corp. UV-530, Rev. 1.00, spectrometer/data system. $Os_3(CO)_{10}(NCMe)_2$, **1**,[17] $PhAuPPh_3$,[18] $2\text{-}NpAuPPh_3$,[19] and $1\text{-}PyrylAuPPh_3$[20] were prepared according to previously reported procedures. Product separations were performed by TLC in air on Analtech 0.25 mm silica gel 60 Å F254 glass plates and Alltech 0.25 mm aluminum oxide UV_{254} glass plates. Due to the small amounts of products, microanalytical data were not obtained.

Synthesis of $Os_3(CO)_{10}(\mu\text{-}C_6H_5)(\mu\text{-}AuPPh_3)$, 2. A 20.6 mg (0.022 mmol) amount of **1** was added to a 100 mL three-neck flask with a solution of 15.5 mg (0.029 mmol) of $PhAuPPh_3$ in 30 mL of methylene chloride. After heating to reflux for 6 h, the solvent was removed *in vacuo*, and the product was then isolated by TLC using a 3:1 hexane/methylene chloride solvent mixture to yield in order of elution 3.8 mg of $Os_3(CO)_{10}(\mu\text{-}Cl)(\mu\text{-}AuPPh_3)$[21] (13% yield) and 14.3 mg of $Os_3(CO)_{10}(\mu\text{-}C_6H_5)(\mu\text{-}AuPPh_3)$, **2** (47%). The $Os_3(CO)_{10}(\mu\text{-}Cl)(\mu\text{-}AuPPh_3)$ may have been formed by the presence of small amounts of $ClAuPPh_3$ present in the $PhAuPPh_3$ reagent. Spectral data for **2**: IR νCO (cm^{-1} in hexane): 2084(m), 2038(vs), 2029(m), 2000(m), 1995(s), 1980(w), 1969(w), 1960(m). ^1H NMR (CD_2Cl_2, 25 °C, TMS): δ 9.62 (d, 1H, Ph), 8.78 (d, 1H, Ph), 8.26 (t, 1H, Ph), 6.97 (t, 1H, Ph), 6.88 (t, 1H, Ph), 7.57−7.47 (m, 15H, PPh_3). $^{31}P\{^1H\}$ NMR (CD_2Cl_2, 25 °C, 85% ortho-H_3PO_4): δ 80.57 (s,1P, P-Au). EI+/MS: m/z 1388 (M^+), 1360 ($M^+ - CO$), 1332 ($M^+ - 2CO$). UV−vis spectra for **2** at 1.05×10^{-4} M in CH_2Cl_2: λ_{max} = 397 nm, ε = 5505 M^{-1} cm^{-1}, λ_{max} = 632 nm, ε = 560 M^{-1} cm^{-1}.

Synthesis of $Os_3(CO)_{10}(2\text{-}C_{10}H_7)(\mu\text{-}AuPPh_3)$, 3. A mixture of 20.8 mg (0.022 mmol) of **1** and 12.8 mg (0.022 mmol) of $2\text{-}NpAuPPh_3$ was stirred in 30 mL of methylene chloride at reflux for 6 h. The solvent was removed *in vacuo*, and the product was then isolated by TLC by using a 3:1 hexane/methylene chloride solvent mixture to yield in order of elution 6.3 mg of $Os_3(CO)_{10}(\mu\text{-}Cl)(\mu\text{-}AuPPh_3)$ (21% yield) and 18.2 mg of $Os_3(CO)_{10}(2\text{-}C_{10}H_7)(\mu\text{-}AuPPh_3)$, **3** (58% yield). The $Os_3(CO)_{10}(\mu\text{-}Cl)(\mu\text{-}AuPPh_3)$[21] may have been formed by the presence of small amounts of $ClAuPPh_3$ present in the $2\text{-}NpAuPPh_3$ reagent. Spectral data for **3**: IR ν_{CO} (cm^{-1} in CH_2Cl_2): 2083(m), 2035(vs), 2024(m), 2002(sh), 1992(s), 1967(w), 1942(sh). ^1H NMR (toluene, 25 °C, TMS): δ 8.65 (dd, 1H, Nap), 8.50 (d, 1H, Nap), 7.85 (d, 1H, Nap), 7.52 (dd, 2H, Nap), 7.25 (d, 1H, Nap), 7.10−6.98 (m, 15H, PPh_3), 6.58 (d, 1H, Nap). $^{31}P\{^1H\}$ NMR (toluene, 25 °C, 85% ortho-H_3PO_4): δ 82.84 (s, 1P, P-Au). EI+/MS: m/z 1438 (M^+), 1410 ($M^+ - CO$), 1382 ($M^+ - 2CO$),1354 ($M^+ - 3CO$). UV−vis spectra for **3** at 2.47×10^{-4} M in CH_2Cl_2: λ_{max} = 391 nm, ε = 8676 M^{-1} cm^{-1}, λ_{max} = 405 nm, ε = 7522 M^{-1} cm^{-1}, λ_{max} = 518 nm, ε = 3009 M^{-1} cm^{-1}.

Reaction of 1 with (1-Pyryl)AuPPh$_3$. A 30.0 mg (0.0276 mmol) amount of **1** was added to a 100 mL three-neck flask with a solution of 20.0 mg (0.0303 mmol) of $(1\text{-}Pyryl)AuPPh_3$ in 30 mL of methylene chloride. The solvent was removed *in vacuo* after refluxing for 6 h, and the product was then isolated by TLC by using a 4:1 hexane/methylene chloride solvent mixture: 1.8 mg of $ClOs_3(CO)_{10}AuPPh_3$ (5% yield), 25.6 mg of $Os_3(CO)_{10}(\mu\text{-}2\text{-}Pyryl)(\mu\text{-}AuPPh_3)$, **4** (61%), and 3.2 mg of $Os_3(CO)_{10}(\mu\text{-}4\text{-}Pyryl)(\mu\text{-}AuPPh_3)$, **5** (8%), were obtained. Spectral data for **4**: IR νCO (cm^{-1} in CH_2Cl_2): 2082(m), 2036(vs), 2028(m), 2001(m), 1992(s), 1962(w). ^1H NMR (CD_2Cl_2, 25 °C, TMS): δ 10.16 (s, 1H, Pyryl), 9.53 (s, 1H, Pyryl), 8.23−7.97 (m, 7H, Pyryl), 7.63−7.50 (m, 15H, PPh_3). $^{31}P\{^1H\}$ NMR (CD_2Cl_2, 25 °C, 85% ortho-H_3PO_4): δ 80.67 (s,1P, P-Au). EI+/MS: m/z 1512 (M^+). Spectral data for **5**: IR νCO (cm^{-1} in CH_2Cl_2): 2082(m), 2036(vs), 2023(m), 2001(m), 1991(s), 1964(w). ^1H NMR ($CDCl_3$, 25 °C, TMS): δ 9.19 (d, 1H, Pyryl), 9.09 (s, 1H, Pyryl), 8.34 (d, 1H, Pyryl), 8.22 (d, 1H, Pyryl), 7.99 (s, 2H, Pyryl), 7.94−7.86 (m, 3H, Pyryl), 7.50−7.44 (m, 15H, PPh_3). $^{31}P\{^1H\}$ NMR ($CDCl_3$, 25 °C, 85% ortho-H_3PO_4): δ 80.48 (s, 1P, P-Au). ES+/MS: m/z 1512 (M^+).

Synthesis of $Os_3(CO)_9(\mu_3\text{-}C_6H_4)(\mu\text{-}AuPPh_3)(\mu\text{-}H)$, 6. To a 50 mL three-neck flask were added 11.8 mg (0.0085 mmol) of **2** and 15 mL of octane. The solution was heated to reflux for 15 min (125 °C). The solvent was removed *in vacuo*, and the product was then isolated by TLC using a 3:1 hexane/methylene chloride solvent mixture. This yielded 10.8 mg of $Os_3(CO)_9(\mu_3\text{-}C_6H_4)(\mu\text{-}AuPPh_3)(\mu\text{-}H)$, **6** (94% yield). Spectral data for **6**: IR ν_{CO} (cm^{-1} in CH_2Cl_2): 2076(w), 2055(vs), 2031(vs), 1998(m), 1982(s), 1948(sh). ^1H NMR (CD_2Cl_2, 25 °C, TMS): δ 7.89 (q, 2H, C_6H_4), 7.59−7.48 (m, 15H, PPh_3), 6.73 (q, 2H, C_6H_4), −20.79 (d, 1H, hydride). $^{31}P\{^1H\}$ NMR (CD_2Cl_2, 25 °C, ref 85% ortho-H_3PO_4): δ 73.05 (s, 1P, P-Au). EI+/MS: m/z 1360(M^+), 1332 ($M^+ - CO$), 1304 ($M^+ - 2CO$), 1276 ($M^+ - 3CO$).

Synthesis of $Os_3(CO)_{10}(\mu_3\text{-}1,2\text{-}\eta^2\text{-}C_{10}H_6)(\mu\text{-}AuPPh_3)(\mu\text{-}H)$, 7. To a 50 mL three-neck flask were added 7.1 mg (0.0049 mmol) of **3** and 10 mL of octane. The solution was heated to reflux for 30 min at 125 °C, and the solvent was removed *in vacuo*. The product was then isolated by TLC by using a pure hexane solvent to yield 0.8 mg of unreacted **3** and 4.3 mg of yellow $Os_3(CO)_{10}(\mu_3\text{-}1,2\text{-}\eta^2\text{-}C_{10}H_6)(\mu\text{-}AuPPh_3)(\mu\text{-}H)$, **7** (63% yield). Spectral data for **7**: IR ν_{CO} (cm^{-1} in CH_2Cl_2): 2075(w), 2053(vs), 2033(vs), 1998(m), 1981 (s), 1952(sh). ^1H NMR (CD_2Cl_2, 25 °C, TMS): δ 7.90 (dd, 1H, $C_{10}H_6$), 7.64 (s, 1H, $C_{10}H_6$), 7.61−7.49 (m, 3H, $C_{10}H_6$, 15H, PPh_3), 6.81 (d, 1H, $C_{10}H_6$), −20.05 (d, 1H, hydride). $^{31}P\{^1H\}$ NMR (CD_2Cl_2, 25 °C, ref 85% ortho-H_3PO_4): δ 75.35 (s, 1P, P-Au). EI+/MS: m/z 1410 (M^+), 1382 ($M^+ - CO$), 1354 ($M^+ - 2CO$), 1326 ($M^+ - 3CO$), 1298 ($M^+ - 4CO$).

Synthesis of $Os_3(CO)_9(AuPPh_3)(\mu_3\text{-}1,2\text{-}Pyryne)(\mu\text{-}H)$, 8, and $Os_3(CO)_9(AuPPh_3)(\mu_3\text{-}4,5\text{-}C_{16}H_9)(\mu\text{-}H)$, 9. To a 50 mL three-neck flask was added 20.0 mg (0.0132 mmol) of **4** into 20 mL of octane. After heating for 30 min at 125 °C, the solvent was removed *in vacuo*, and the product was then isolated by TLC by using a 6:1 hexane/methylene chloride solvent mixture. This yielded 17.1 mg (87% yield) of a mixture of $Os_3(CO)_{10}(\mu\text{-}AuPPh_3)(\mu\text{-}Pyryne)(\mu\text{-}H)$, **8**, and $Os_3(CO)_9(\mu\text{-}AuPPh_3)(\mu_3\text{-}4,5\text{-}C_{16}H_9)(\mu\text{-}H)$, **9**. Compounds **8** and **9** could not be completely separated chromatographically. Pure crystalline forms of **8** and **9** were obtained by cutting the top (**8**) and bottom (**9**) edges of the broad band obtained from a 0.25 mm alumina TLC plate and then recrystallizing from hexane solutions. The ratio of compounds **8** and **9** in the initial mixture was 43/57 based on the integration of the corresponding hydride peaks in the ^1H NMR spectrum. Spectral data for **8**: IR ν_{CO} (cm^{-1} in CH_2Cl_2): 2074(w), 2053(s), 2038(vs), 2001(m), 1988(m), 1978(m), 1956(sh). ^1H NMR (CD_2Cl_2, 25 °C, TMS): δ 8.40 (s, 1H, $C_{16}H_8$), 8.24 (d, 1H, $C_{16}H_8$), 8.18 (d, 1H, $C_{16}H_8$), 8.09 (t, 1H, $C_{16}H_8$), 7.87 (dd, 2H, $C_{16}H_8$), 7.67 (d, 1H, $C_{16}H_8$), 7.63−7.51 (m, 1H, $C_{16}H_8$, 15H, PPh_3), −19.75 (d, 1H, hydride). $^{31}P\{^1H\}$ NMR (CD_2Cl_2, 25 °C, ref 85% ortho-H_3PO_4): δ 74.26 (s, 1P, P-Au). EI+/MS: m/z 1484 (M^+), 1456 ($M^+ - CO$), 1428 ($M^+ - 2CO$), 1400 ($M^+ - 3CO$), 1372

($M^+ - 4CO$), 1344 ($M^+ - 5CO$). Spectral data for **9**: IR ν_{CO} (cm^{-1} in CH_2Cl_2): 2073(w), 2052(s), 2038(vs), 2001(m), 1989(w), 1979(m), 1957(w). ^1H NMR (CD_2Cl_2, 25 °C, TMS): δ 8.00 (dd, 2H, $C_{16}H_8$), 7.97 (dd, 2H, $C_{16}H_8$), 7.90 (s, 2H, $C_{16}H_8$), 7.81 (t, 2H, $C_{16}H_8$) 7.56−7.42 (m, 15H, PPh_3), −18.90 (d, 1H, hydride). $^{31}P\{^1H\}$ NMR (CD_2Cl_2, 25 °C, ref 85% ortho-H_3PO_4): δ 78.03 (s, 1P, P-Au). EI+/MS: m/z 1484 (M^+), 1456 ($M^+ - CO$), 1428 ($M^+ - 2CO$), 1400 ($M^+ - 3CO$), 1372 ($M^+ - 4CO$), 1344 ($M^+ - 5CO$).

Crystallographic Analyses. Green crystals of **2**, green crystals of **3a**, green crystals of **4**, orange crystals of **6**, and yellow crystals of **7** suitable for X-ray diffraction analyses were all obtained by slow evaporation of solvent from a solution in pure hexane at 25 °C. Red crystals of **3b**, black crystals of **5**, red crystals of **8**, and orange crystals of **9** were obtained by cooling a solution of the pure compound in hexane solvent to −25 °C. X-ray intensity data were measured by using a Bruker SMART APEX CCD-based diffractometer with Mo Kα radiation (λ = 0.71073 Å). The raw data frames were integrated with the SAINT+ program by using a narrow-frame integration algorithm.[22] Corrections for Lorentz and polarization effects were also applied by using SAINT+. Empirical absorption corrections based on the multiple measurement of equivalent reflections were applied by using the program SADABS for each structural analysis. All of the structures were solved by a combination of direct methods and difference Fourier syntheses and were refined by full-matrix least-squares on F^2 by using the SHELXTL software package.[23] Crystal data, data collection parameters, and results of the analyses are available in the Supporting Information; see Table S1.

Computational Analyses. For the calculations on **2**, geometry-optimized calculations were performed with the ADF2012 program[24] by using the PBEsol functional[24] with scalar relativistic correction and valence quadruple-ζ + 4 polarization, relativistically optimized (QZ4P) basis sets for osmium and gold, and valence double-ζ function (DZ) basis sets for the phosphorus, carbon, oxygen, and hydrogen atoms with no frozen cores. The molecular orbitals for **2** and their energies were determined by geometry-optimized calculations that were initiated with the structures as determined from the crystal structure analyses. The fragment analysis for **2** was also performed with the ADF programs by using the meta-generalized gradient approximation (meta-GGA) level nonempirical Tao−Perdew−Staroverov−Scuseria (TPSS) functional.[25] The phenyl group was used as one fragment, and the other fragment was the complete molecule minus the phenyl group. The MOs of the fragments were then calculated by using the same basis sets as described above.

For the calculations of **3b**, geometry-optimized calculations were performed with the ADF2012 program[24] by using the PBEsol functional with scalar relativistic correction and valence triple-ζ + polarization, relativistically optimized (TZP) basis sets, with small frozen cores. The molecular orbitals and their energies were determined by geometry optimization calculations that were initiated with the structures as determined from the crystal structure analyses, except for **3b**, where PMe_3 was substituted for the PPh_3 ligand to simplify these calculations.

RESULTS AND DISCUSSION

Compound **1** reacts with $C_6H_5Au(PPh_3)$ in CH_2Cl_2 at 40 °C by elimination of its NCMe ligands and an oxidative-addition of the Au−C bond of the $C_6H_5Au(PPh_3)$ to the $Os_3(CO)_{10}$ group to yield the complex $Os_3(CO)_{10}(\mu\text{-}C_6H_5)(\mu\text{-}AuPPh_3)$, **2**, in 47% yield. The structure of **2** was established crystallographically, and an ORTEP diagram of its molecular structure is shown in Figure 1. The molecule contains a triangular cluster of three osmium atoms with a η^1-bridging phenyl ligand and a bridging $AuPPh_3$ group across the Os1−Os2 bond. The plane of the C_6-ring is nearly perpendicular, 86.9(3)°, to the plane of the Os_3 triangle. The bond distances to the carbon atom C(1) of the bridging phenyl group, Os1−C1 = 2.191(13) Å and Os2−C1 = 2.236(11) Å, are slightly shorter on average than those found in two previously reported triosmium cluster complexes containing η^1-bridging phenyl ligands: $Os_3(CO)_8(\mu_3\text{-}Se_2)(\mu\text{-}Ph)(\mu\text{-}PhC{=}O)$,[26] 2.24(2) and 2.51(2) Å, and $Os_3(CO)_8(\mu\text{-}PPh_2)(\mu\text{-}Ph)(\mu\text{-}PPhC_6H_4)$,[5a] 2.19 and 2.39 Å.

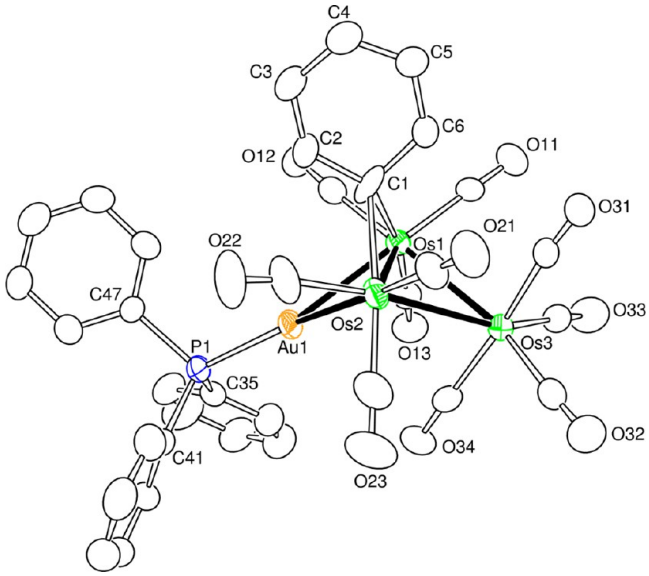

Figure 1. ORTEP diagram of the molecular structure of $Os_3(CO)_{10}(\mu\text{-}C_6H_5)(\mu\text{-}AuPPh_3)$, **2**, showing 30% thermal ellipsoid probability. The hydrogen atoms are omitted for clarity. Selected interatomic bond distances (Å) and angles (deg) are as follows: Os1−Os2 = 2.7521(6), Os1−Os3 = 2.8785(5), Os2−Os3 = 2.8746(5), Os1−C1 = 2.191(13), Au1−Os1 = 2.7621(5), Au1−Os2 = 2.7668(5), Os2−C1 = 2.236(11); Os1−C1−Os2 = 76.9(4).

The doubly bridged Os1−Os2 bond in **2** is also shorter, 2.7521(6) Å, than the two other Os−Os bonds, Os1−Os3 = 2.8785(5) Å and Os2−Os3 = 2.8746(5) Å, in the complex. Assuming that the phenyl ligand and the $Au(PPh_3)$ group are both one-electron donors, then compound **2** contains a total of only 46 electrons at the metal atoms and is formally unsaturated. Compound **2** is electronically similar to the 46-electron triosmium cluster complexes $Os_3(CO)_{10}(\mu\text{-}H)_2$,[15,27] $Os_3(CO)_8(\mu\text{-}AuPEt_3)_2$,[28] and $Os_3(CO)_8(\mu\text{-}AuPPh_3)(\mu\text{-}H)$,[29] for which their doubly bridged Os−Os bond distances are 2.683(1), 2.684(1), and 2.699(1) Å, respectively. The unsaturation in **2** is manifested in a delocalized bonding across the Os(1), Os(2), and C(1) atoms. In order to understand the nature of the bonding of the bridging phenyl ligand to the metal atoms, a DFT molecular orbital analysis was performed. Selected molecular orbitals that show the bonding of the bridging phenyl ring to the metal atoms are shown in Figure 2. The most important of these are the HOMO−3, HOMO−5, HOMO−14, and HOMO−18.

To understand the origin of these orbitals, a fragment analysis was performed. The complex was divided into two fragments: (1) the phenyl ring and (2) the $Os_3(CO)_{10}(\mu\text{-}AuPPh_3)$ group. A molecular energy level diagram showing the MOs of the fragments and the most important orbitals involved in the bonding of the ring to the metal atoms is shown in Figure 3.

The HOMO−14 is a combination of the singly occupied MO (SOMO) of the phenyl ring fragment and the singly occupied MO of the $Os_3(CO)_{10}(\mu\text{-}AuPPh_3)$ fragment. The SOMO of the phenyl ring is the orbital that would be σ-bonded to a hydrogen atom for the formation of benzene. The HOMO−14 serves as the basis for what would commonly be viewed as a Os−C−Os, three-center, two-electron σ-bond. The LUMO of the $Os_3(CO)_{10}(\mu\text{-}AuPPh_3)$ fragment interacts with the π-HOMO−1 of the ring to form the strong bonding HOMO−

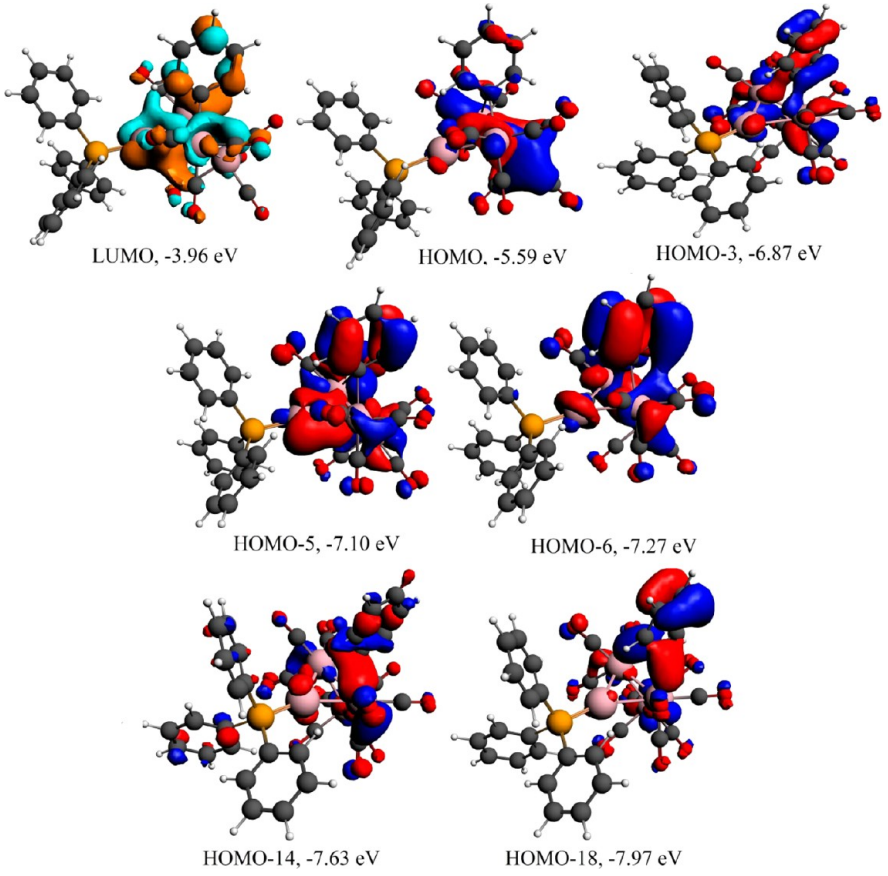

Figure 2. Selected molecular orbital diagrams of the LUMO, HOMO, HOMO−3, HOMO−5, HOMO−6, HOMO−14, and HOMO−18 with calculated energies showing the bonding of the η^1-bridging phenyl ligand to the osmium atoms in **2**.

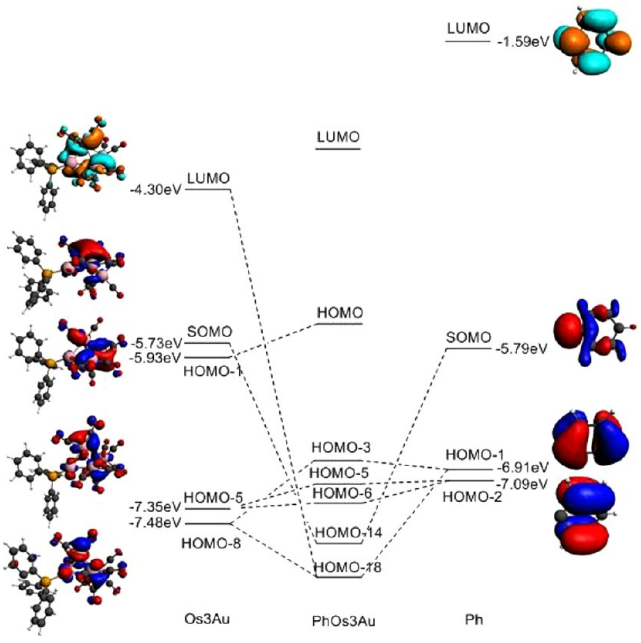

Figure 3. An energy level diagram of the molecular orbitals with calculated energies from fragment analysis showing the origin of the MOs in Figure 2 for compound **2**.

18 of **2**, which can be viewed as π-donation from the ring to the cluster. This π-donation from the ring helps to reduce the electronic unsaturation in **2**. Such π-donation is not available to molecules such as $Os_3(CO)_{10}(\mu\text{-}H)_2$, and this helps to explain why the Os−Os bond distance in **2** is significantly longer than that in $Os_3(CO)_{10}(\mu\text{-}H)_2$. Our calculations revealed no significant bonding interactions between the metal atoms and the unoccupied π-orbitals of the phenyl ring; that is, there was no significant π-back-bonding to the ring. One reason for this is because the ring π^*-orbitals lie at too high an energy. For example, the lowest unoccupied molecular orbital (LUMO) of the ring lies at −1.59 eV; see Figure 3.

The reaction of **1** with 2-NpAu(PPh_3) yielded the complex $Os_3(CO)_{10}(\mu\text{-}2\text{-}Np)(\mu\text{-}AuPPh_3)$, **3**, in 58% yield. Unlike **2**, solutions of **3** are pink. However, crystals grown from hexane solutions at room temperature were green and similar in color to those obtained for **2**. Most interestingly, crystals of **3** grown from hexane at −25 °C were pink in color. Hereafter the green crystals shall be called **3a** and the pink ones **3b**, because they are isomers; see below. The molecular structures of **3a** and **3b** were established crystallographically.

An ORTEP diagram of the molecular structure of **3a** is shown in Figure 4. The structure of **3a** is similar to that of **2** except that it contains an η^1-2-Np ligand that bridges the $AuPPh_3$-bridged Os−Os bond, Os1−C1 = 2.313(11) Å and Os2−C1 = 2.332(11) Å. As in **2**, the plane of the C_{10}-ring is virtually perpendicular to the plane of the Os_3 triangle. Assuming the 2-Np ligand and the $AuPPh_3$ group serve as one-electron donors, then compound **3a** contains 46 electrons and is unsaturated just like **2**. Accordingly, the Os1−Os2 bond is short, 2.7484(6) Å, compared to the other Os−Os bonds: Os1−Os3 = 2.8745(6) Å; Os2−Os3 = 2.8668(6) Å.

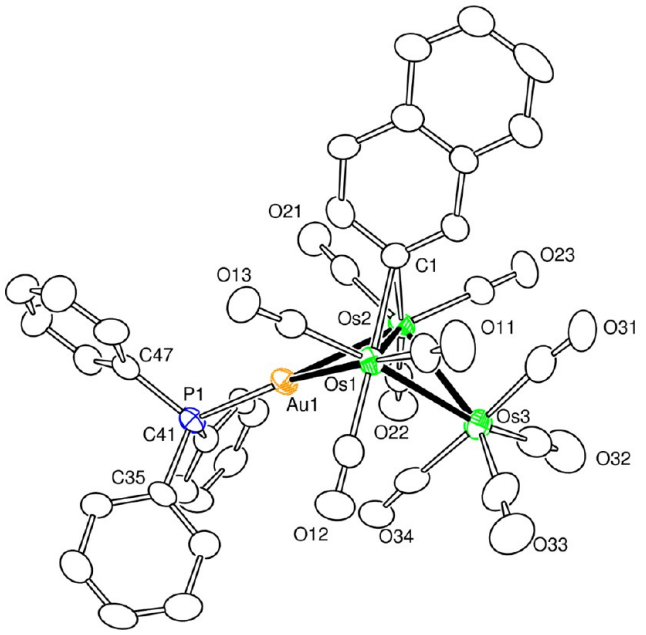

Figure 4. ORTEP diagram of the molecular structure of $Os_3(CO)_{10}(\mu$-2-Np$)(\mu$-AuPPh$_3$), **3a**, obtained from the green crystals showing 30% thermal ellipsoid probability. The hydrogen atoms are omitted for clarity. Selected interatomic bond distances (Å) are as follows: Os1−Os2 = 2.7484(6), Os1−Os3 = 2.8745(6), Os2−Os3 = 2.8668(6), Au1−Os1 =2.7424(6), Au1−Os2 = 2.7772(6), Os1−C1 = 2.313(11), Os2−C1 = 2.332(11).

An ORTEP diagram of the molecular structure of **3b** is shown in Figure 5. This structure is an isomer of **3a** in that it contains an η^2-2-Np ligand that bridges the AuPPh$_3$-bridged Os−Os bond. The naphthyl atom C(1) is bonded to both osmium atoms, Os1−C1 = 2.313(11) Å and Os2−C1 = 2.332(11) Å, but the naphthyl atom C(6) is also bonded to Os(2), Os2−C6 = 2.544(10) Å, although the distance is significantly longer. As a result, the plane of the planar C_{10}-ring is not perpendicular to the Os_3 triangle. The plane is actually 49.3(3)° from the plane of the Os_3 triangle. The C1−C6 distance is 1.380(14) Å. In this molecule the 2-Np ligand serves as a three-electron donor of the type **C**.

The AuPPh$_3$ group serves as a one-electron donor, and the osmium atoms in the pink isomer **3b** contain a total of 48 electrons. The triosmium cluster is electronically saturated, and as a result, there is no unusually short Os−Os bond in **3b**. The doubly bridged Os1−Os2 bond, 2.8538(6) Å, is nearly as long as the other two Os−Os bonds: Os1−Os3 = 2.8997(6) Å and Os2−Os3 = 2.8899(7) Å. Because the complex is electronically saturated, the HOMO/LUMO gap in **3b** is larger than that in **2** and the absorption in the visible spectrum lies at higher energy, λ = 518 nm, ε = 3009 cm^{-1} M^{-1}, which accounts for its pink color in solution. The structure **3b** evidently converts to **3a** when crystals are grown at room temperature. We have not yet obtained any spectroscopic evidence for the presence of the **3a** isomer in solutions at room temperature.

The reaction of **1** with 1-PyrylAu(PPh$_3$) provided the product $Os_3(CO)_{10}(\mu$-2-Pyryl$)(\mu$-AuPPh$_3$), **4**, in 61% yield. Like **2**, the color of **4** is green in solution. Interestingly, however, there was also a second product, $Os_3(CO)_{10}(\mu$-4-Pyryl$)(\mu$-AuPPh$_3$), **5**, formed in low yield (8%), which is brown. The molecular structures of **4** and **5** were both established by crystallographic methods.

An ORTEP diagram of the molecular structure of **4** is shown in Figure 6. The structure of **4** is similar to that of **2** and **3a** except that it contains an η^1-2-Pyryl ligand that bridges the AuPPh$_3$-bridged Os−Os bond: Os1−C35 = 2.291(12) Å and Os2−C35 =

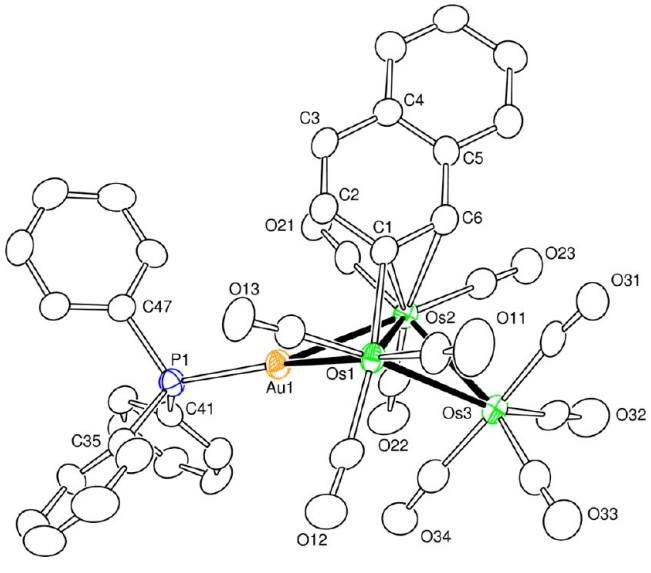

Figure 5. ORTEP diagram of the molecular structure of $Os_3(CO)_{10}(\mu_3$-η^2-2-Np$)(\mu$-AuPPh$_3$), **3b**, showing 30% thermal ellipsoid probability. The hydrogen atoms are omitted for clarity. Selected interatomic bond distances (Å) are as follows: Os1−Os2 = 2.8538(6), Os1−Os3 = 2.8997(6), Os2−Os3 = 2.8899(7), Au1−Os1 = 2.7573(6), Au1−Os2 = 2.8146(6), Os1−C1 = 2.174(11), Os2−C1 = 2.369(10), Os2−C6 = 2.544(10), C1−C6 = 1.380(14).

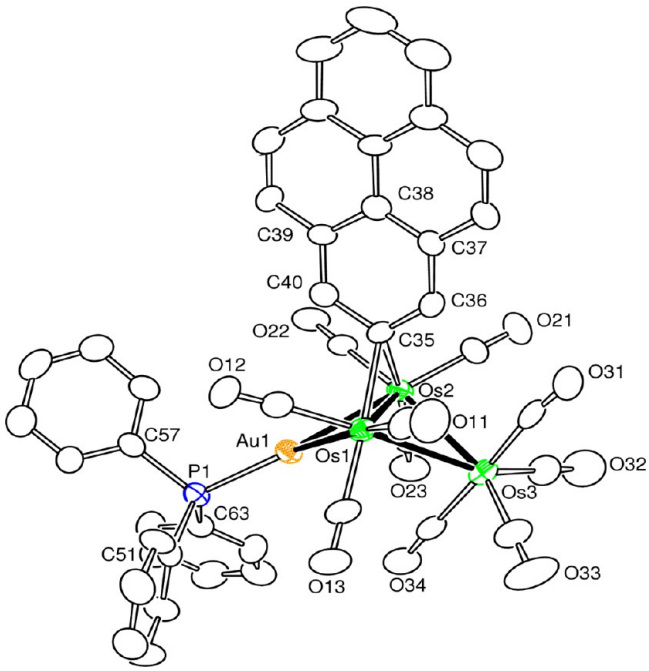

Figure 6. ORTEP diagram of the molecular structure of $Os_3(CO)_{10}(\mu$-2-Pyryl$)(\mu$-AuPPh$_3$), **4**, showing 30% thermal ellipsoid probability. Selected interatomic bond distances (Å) and angles (deg) are as follows: Au1−Os1 = 2.7515(7), Au1−Os2 = 2.7518(7), Os1−Os2 = 2.7485(7), Os1−Os3 = 2.8980(7), Os2−Os3 = 2.8863(7), Os1−C35 = 2.291(12), Os2−C35 = 2.345(13).

2.345(13) Å. Similarly to **2** and **3a**, the plane of the C_{16}-ring is virtually perpendicular to the plane of the Os_3 triangle. The interplanar angle is 86.9(1)°. If the 2-Pyryl ligand and the $AuPPh_3$ group serve as one-electron donors, then compound **4** contains a total of 46 valence electrons and is unsaturated just like **2** and **3a**. Accordingly, the Os1−Os2 bond is short, 2.7485(7) Å, compared to the other Os−Os bonds, Os1−Os3 = 2.8980(7) Å and Os2−Os3 = 2.8863(7) Å.

An ORTEP diagram of the molecular structure of **5** is shown in Figure 7. This compound is an isomer of **4**, and it contains an η^1-4-Pyryl ligand that bridges the $AuPPh_3$-bridged Os−Os bond, Os1−C47 = 2.247(17) Å and Os2−C47 = 2.364(18) Å. In **5**, the plane of the planar C_{16}-ring is not exactly perpendicular to the Os_3 triangle. The interplanar angle is 75.3(1)°. The η^1-4-Pyryl ligand and the $AuPPh_3$ group in **5** both serve as a one-electron donor, and therefore the metal atoms in **5** contain a total of 46 electrons, indicating that it is also unsaturated like **2**, **3a**, and **4**. The unsaturated, η^1-4-Pyryl, doubly bridged Os1−Os2 bond, 2.7789(10) Å, is slightly longer than the η^1-2-Pyryl-bridged bond found in **4**, and Os1−Os3 = 2.9313(12) Å and Os2−Os3 = 2.8897(11) Å. Interestingly, by following the ^{1}H NMR spectra, we found that compound **4** can be partially converted to compound **5** by heating to 40 °C in a solution in CH_2Cl_2 solvent for 48 h. We have not yet established a mechanism for the hydrogen shift for the transformation of **4** and **5**.

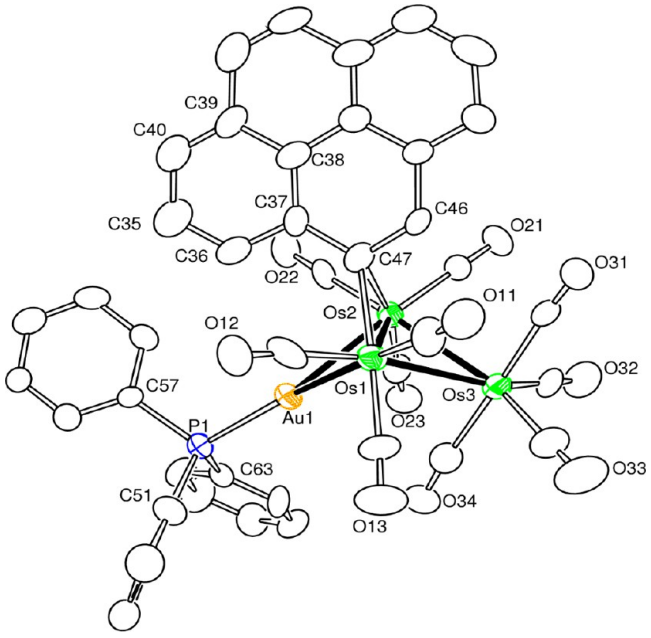

Figure 7. ORTEP diagram of the molecular structure of $Os_3(CO)_{10}$(4-Pyryl)(μ-$AuPPh_3$), **5**, showing 30% thermal ellipsoid probability. Selected interatomic bond distances (Å) and angles (deg) are as follows: Au1−Os1 = 2.7618(10), Au1−Os2 = 2.7945(10), Os1−Os3 = 2.9313(12), Os1−Os2 = 2.7789(10), Os2−Os3 = 2.8897(11), Os1−C47 = 2.247(17), Os2−C47 = 2.364(18), Os1−C47−Os2 = 74.1(5).

When compound **2** was heated to reflux in a solution of octane solvent (125 °C), it was decarbonylated and transformed into the compound $Os_3(CO)_9(\mu_3\text{-}C_6H_4)(\mu\text{-}AuPPh_3)(\mu\text{-}H)$, **6**, in 94% yield. Compound **6** was characterized crystallographically, and an ORTEP diagram of its molecular structure is shown in Figure 8. Compound **6** contains a triply bridging C_6H_4 "benzyne" ligand. The structure of **6** is similar to that of $Os_3(CO)_9(\mu_3\text{-}C_6H_4)(\mu\text{-}H)_2$ except for the presence of the bridging $AuPPh_3$ in place of one of the bridging hydride ligands.[9] The benzyne C−C bond distance, C1−C2 = 1.429(14) Å, is typical of those observed for other benzyne ligands, e.g., 1.45(5) and 1.64(6) Å for $Os_3(CO)_9(\mu_3\text{-}C_6H_4)(\mu\text{-}H)_2$.[9,10] Compound **6** was formed by the loss of a CO ligand from the $Os(CO)_4$ group in **2** and the activation of one of the ortho-positioned CH bonds in the bridging phenyl ligand. The benzyne ligand serves as a four-electron donor, and the complex is electronically saturated with a total of 48 valence electrons at the metal atoms.

When a solution of **3** was heated to reflux in octane solvent, it was decarbonylated and transformed into the compound $Os_3(CO)_9(\mu_3\text{-}C_{10}H_6)(\mu\text{-}AuPPh_3)(\mu\text{-}H)$, **7**, in 63% yield. Compound **7** was also characterized crystallographically, and an ORTEP diagram of its molecular structure is shown in Figure 9. The structure of **7** is similar to that of **6**. Compound **7** contains a triply bridging 1,2-naphthyne ligand. Complexes containing naphthyne ligands are exceedingly rare.[30] The naphthyne C−C bond distance (C1−C6 = 1.435(16) Å) is similar in length to that found in the benzyne ligand in **6**. The Au- and H-bridged bonds (Os1−Os2 = 2.8950(6) Å, Os1−Os3 = 2.9882(7) Å) are longer than the remaining Os−Os bond (Os2−Os3 = 2.7494(6) Å). The naphthyne ligand in **7** is a four-electron donor. The metal atoms thus contain a total of 48 electrons and are electronically saturated.

DFT computational analyses were performed in order to establish the mechanism of the naphthyne formation and the C−H activation steps. The calculation was initiated by removing one of the axial CO ligands cis to the napthyl ligand from the $Os(CO)_4$ in **3b**. Removal of the other CO ligands did not proceed to the observed product **7** with our optimization refinements. This will be called the CO dissociation mechanism, mechanism 1. Intermediate and ground-state structures were determined by using full geometry optimization. The approximate transition states were computed as maxima of total energy along the reaction coordinate with full geometry optimization of all other coordinates. The energy of the decarbonylated form of **3b** lies about +52 kcal/mol above the ground state **3b**, as shown in the energy profile in Figure 10. This is due to the generation of a vacant site on Os3. Although this may seem high, thermochemical measurements have shown the Os−CO bond strength in $Os_3(CO)_{12}$ is approximately 201 kJ/mol (48 kcal/mol).[31] We think that the Os−CO bond strengths in **3b** should be similar to those in $Os_3(CO)_{12}$ and thus support our calculated results.

As the refinement starts, the naphthyl group moves toward Os3, which contains the vacant binding site. The intermediate **ISS** is formed. In this intermediate, there is an agostic interaction between the ortho-CH bond in the naphthyl group and Os3. The computed structure of this intermediate is shown in Figure 11 (left). The bond distances, Os3−C6 = 2.37 Å, Os3 − H6 = 1.82 Å, and C3−H6 = 1.21 Å, indicate that there are significant Os−C and Os−H interactions and the CH bond is weakened.

The HOMO−13 of this intermediate shows the CH−Os interaction. Since the vacant site has been filled by the two electrons from the CH bond, the energy dropped from +52 kcal/mol above the ground state to +21.42 kcal/mol above the ground state. As the process continues, the CH bond in the intermediate is cleaved via a small transition state (**TS**), which contains a terminally coordinated hydride ligand. The **TS** is located by a geometry scan from the final product **7** to the intermediate, by using the C6···H6 distance as a reaction (scan) coordinate, and fully optimizing all other coordinates. The energy profile along the scan coordinate shows a single well-defined maximum, which

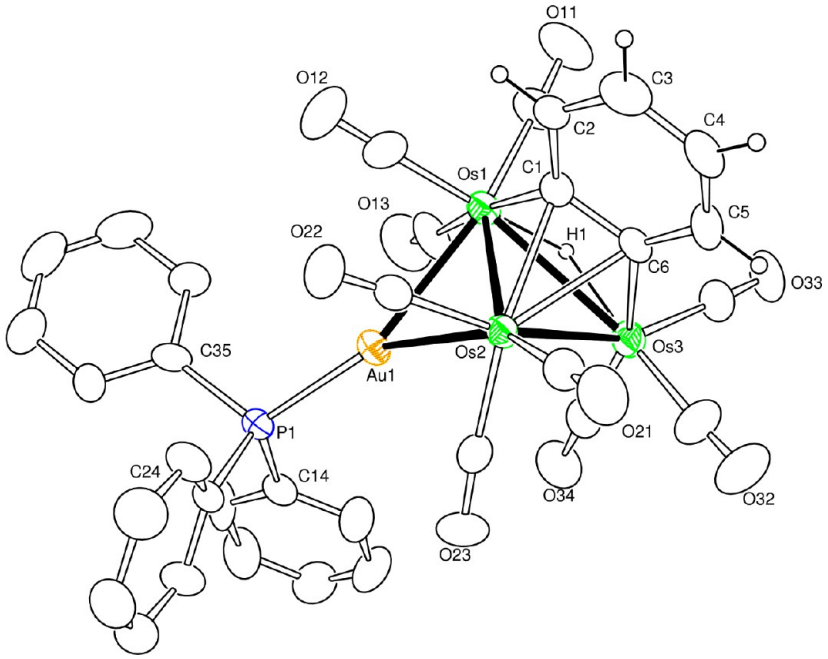

Figure 8. ORTEP diagram of the molecular structure of $Os_3(CO)_9(\mu_3\text{-}\eta^2\text{-}C_6H_4)(\mu\text{-}AuPPh_3)(\mu\text{-}H)$, **6**, showing 30% thermal ellipsoid probability. The hydrogen atoms are omitted for clarity. Selected interatomic bond distances (Å) are as follows: Os1−Os2 = 2.8902(6), Os1−Os3 =3.0229(7), Os2−Os3 = 2.7560(6), Au1−Os1 =2.7507(6), Au1−Os2 = 2.8131(6), Os1−C1 = 2.085(10), Os3−C6 = 2.097(10), Os2−C1 = 2.285(10), Os2−C6 = 2.374(10), Os1−H1 = 1.69(9), Os3−H1 = 1.99(9), C1−C6 = 1.429(14).

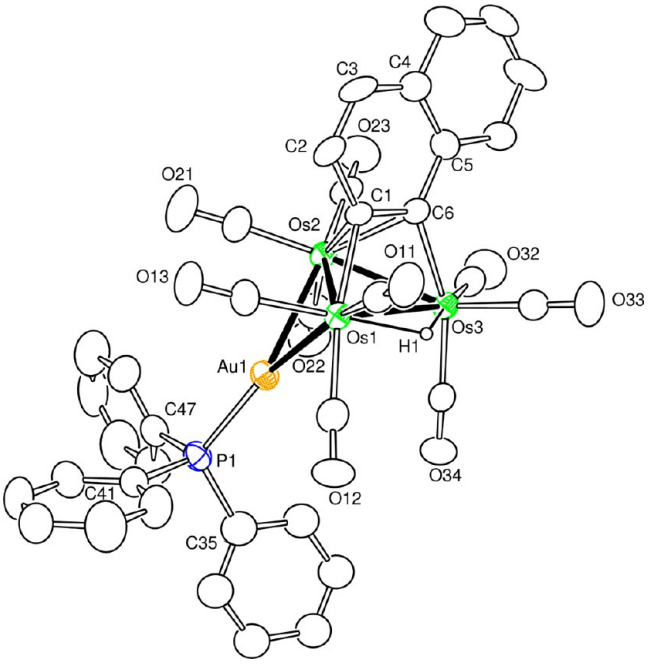

Figure 9. ORTEP diagram of the molecular structure of $Os_3(CO)_{10}(\mu_3\text{-}1,2\text{-}\eta^2\text{-}C_{10}H_6)(\mu\text{-}AuPPh_3)(\mu\text{-}H)$, **7**, showing 30% thermal ellipsoid probability. The hydrogen atoms are omitted for clarity. Selected interatomic bond distances (Å) are as follows: Os1−Os2 = 2.8950(6), Os1−Os3 = 2.9882(7), Os2−Os3 = 2.7494(6), Os1−C1 = 2.123(11), Os2−C1 = 2.298(11), Os2−C6 = 2.370(12), Os1−Au1 = 2.7395(7), Os2−Au1 = 2.7923(7), Os3−C6 = 2.085(12), Au1−P1 = 2.284(3), C1−C6 = 1.435(16).

is called the **TS**. The geometry of this **TS** is shown in Figure 12. The distance between carbon and hydrogen atoms, C6···H6 = 2.06 Å, clearly indicates that the CH bond has been cleaved.

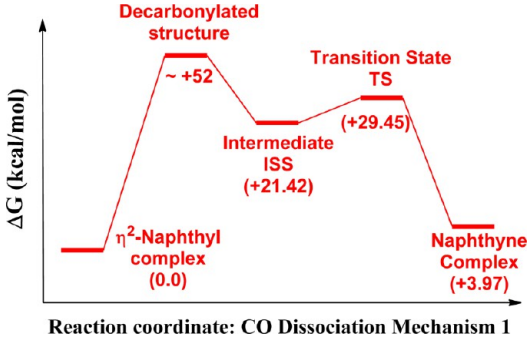

Figure 10. Calculated energy profile showing the decarbonylation and CH activation in the transformation of the naphthyl ligand in **3b** into the naphthyne ligand in **7**, mechanism 1.

The HOMO of **TS** shows hydrogen−osmium bonding. The hydride ligand then shifts to a bridging position across the neighboring metal−metal bond to complete the transformation to **7**. A complete energy profile along the computed reaction coordinate is shown in Figure 10. The ground state of the naphthyne complex is +3.9 kcal/mol higher than that of **3b**. This is mainly because **3b** contains one more carbonyl ligand to stabilize it.

An alternative mechanism was also investigated by performing a scan of the naphthyl carbon−Os(3) distance from its equilibrium value of 3.8 Å down to 1.8 Å, with optimization of all other coordinates, and without removing a CO ligand in advance; see Scheme 1. This mechanism will be called the metal−metal bond-opening mechanism 2. The transition state **TS1** was formed (+47.5 kcal), which contained an agostic interaction of the ortho-positioned CH bond to Os(3).

In the process one of the CO ligands on Os(3) was shifted into a bridging position between atoms Os(2) and Os(3). This structure subsequently settled into a stable intermediate (I1)

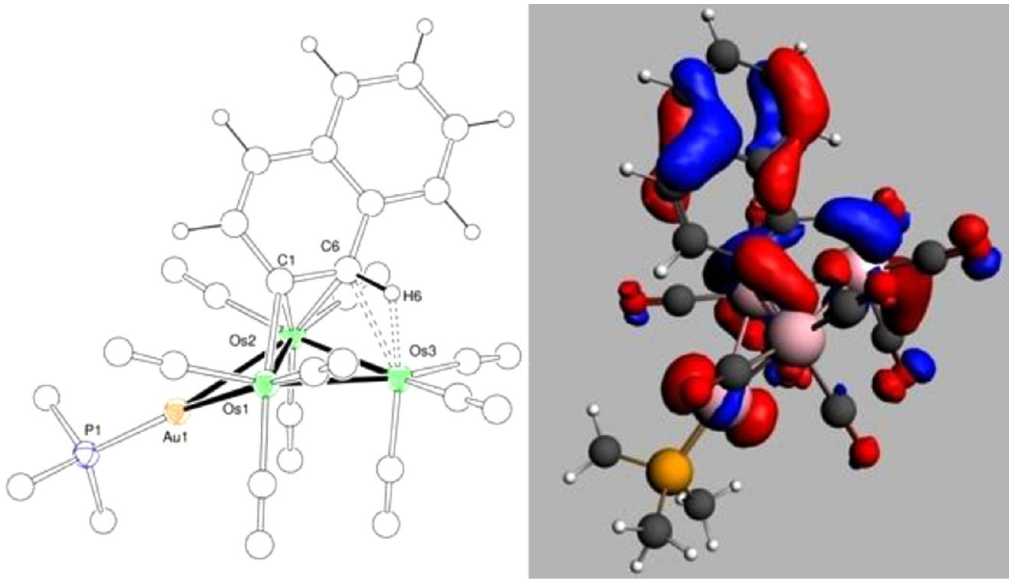

Figure 11. Computed intermediate **ISS** en route to the naphthyne ligand in **7** shows the agostic interaction between the ortho-CH bond in the naphthyl group and the third osmium atom (left). The HOMO−13 of this intermediate shows the bonding of the hydrogen atom H(6) to the osmium (right).

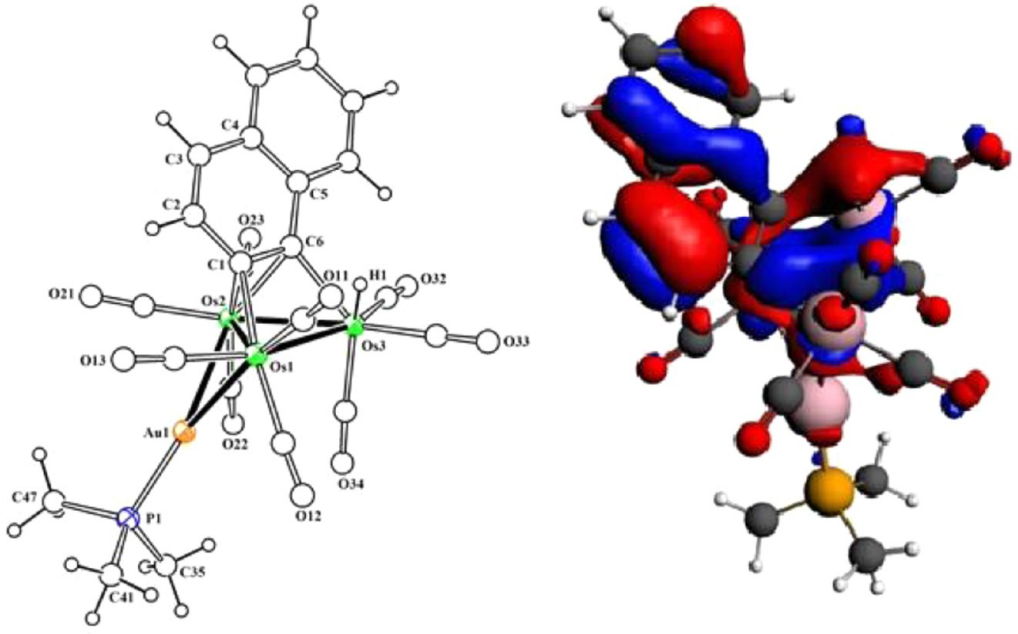

Figure 12. Computed transition state **TS** of the naphthyne formation shows the cleavage of the C−H bond (left). The HOMO of this transition state shows hydrogen−osmium bonding (right).

Scheme 1

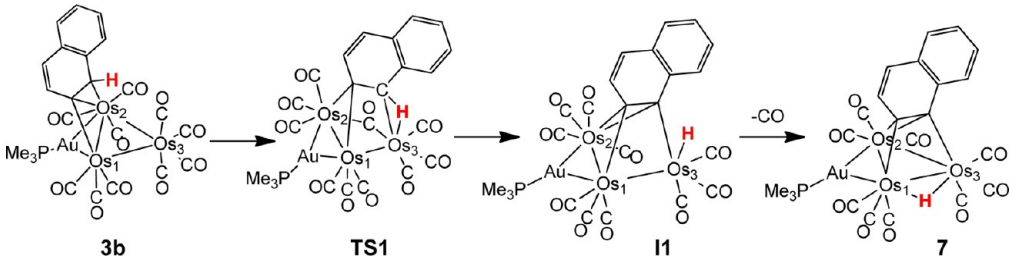

(+38.8 kcal) by shifting the bridging CO ligand to a terminal position on Os(2) and cleaving the Os(2)−Os(3) bond. Simultaneously, the agostic CH bond on the naphthyl ligand was cleaved to form a naphthyne ligand and a terminal hydride ligand. To complete the transformation to **7**, one of the CO ligands on Os2 had to be forcibly removed by scanning the OC−

dx.doi.org/10.1021/om4007399 | *Organometallics* 2013, 32, 6368−6378

Os bond distance from 1.97 to 4.0 Å. In this process a second transition state, **TS2**, was traversed (+64.7 kcal/mol), which finally led to **7** by formation of a metal−metal bond between Os(2) and Os(3) and a shift of the hydride ligand to a bridging position. Although the bond-opening mechanism ultimately produces the correct product, **7**, the barrier of +64.7 kcal/mol is significantly higher than +52 kcal of the original reaction mechanism 1, and for this reason mechanism 1 is considered to be the most likely mechanism.

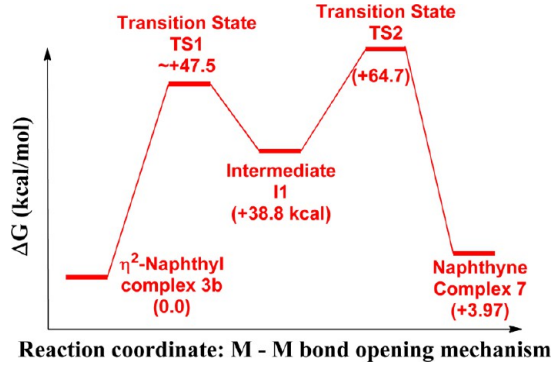

Figure 13. Calculated energy profile showing the CH activation and CO decarbonylation steps in the transformation of the naphthyl ligand in **3b** into the naphthyne ligand in **7** via the metal−metal bond-opening mechanism, mechanism 2.

When a solution of the 2-pyryl complex **4** was heated to reflux in octane solvent, it was decarbonylated and transformed into two new compounds, **8** and **9**, in a combined yield of 87%. Compounds **8** and **9** are isomers, and they are difficult to separate in pure forms. The ratio of compound **8** and **9** in the initial mixture was 43/57 based on the integration of the corresponding hydride peaks in a ^{1}H NMR spectrum. However, they were both crystallized in pure forms and were both characterized by single-crystal X-ray diffraction analyses. An ORTEP diagram of the molecular structure of **8** is shown in Figure 14.

The structure of **8** is similar to that of **6** and **7**, except that it contains a triply bridging 1,2-pyryne ligand coordinated to the cluster. The pyryne C−C bond distance (C35−C36 = 1.435(12) Å) is similar in length to that found for the benzyne and naphthyne ligands found in **6** and **7**, respectively. The Au- and H-bridged bonds (Os1−Os2 = 2.8799(5) Å, Os1−Os3 = 3.0044(5) Å) are longer than the third Os−Os bond (Os2−Os3 = 2.7525(5) Å). The pyryne ligand in **8** is a four-electron donor, and the metal atoms thus contain a total of 48 electrons and are electronically saturated. An ORTEP diagram of the molecular structure of **9** is shown in Figure 15.

The pyryne ligand in **9** is coordinated to the cluster at its 4 and 5 positions, which is similar to that of a previously reported pyryne compound, $Os_3(CO)_9(\mu_3\text{-}4,5\text{-}C_{16}H_9)(\mu\text{-}H)_2$, except for the presence of the bridging $AuPPh_3$ in place of one of the bridging hydride ligands.[32] The pyryne C−C bond distance (C46−C47 = 1.419(9) Å) is similar in length to that found in the aryne ligand in **6**, **7**, and **8**. The Au- and H-bridged bonds (Os1−Os2 = 2.8777(4) Å, Os1−Os3 = 2.9702(4) Å) are longer than the remaining Os−Os bond (Os2−Os3 = 2.7634(4) Å). The pyryne ligand in **9** is also a four-electron donor, and the metal atoms thus contain a total of 48 electrons and are electronically saturated.

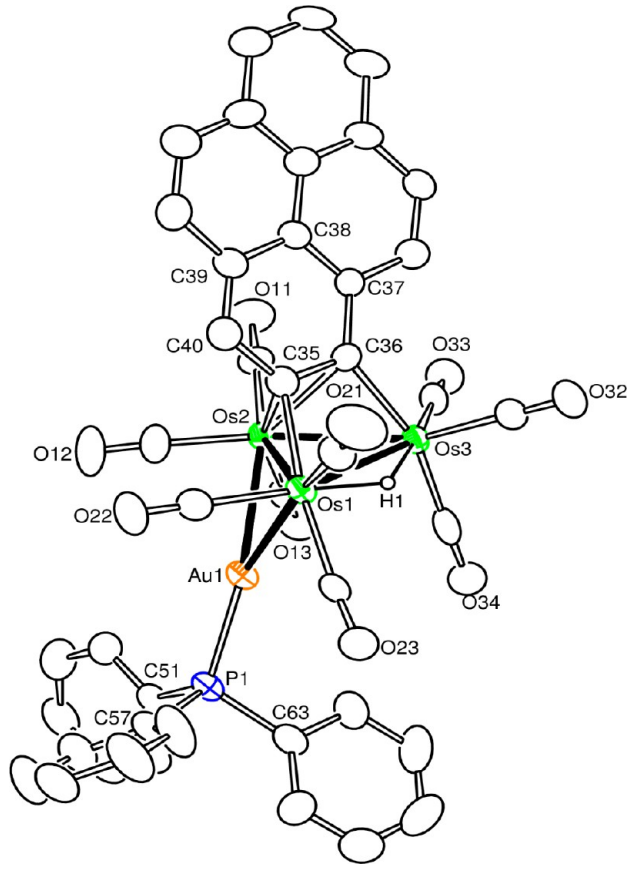

Figure 14. ORTEP diagram of the molecular structure of $Os_3(CO)_{10}(\mu_3\text{-}1,2\text{-pyryne})(\mu\text{-}AuPPh_3)(\mu\text{-}H)$, **8**, showing 30% thermal ellipsoid probability. The hydrogen atoms are omitted for clarity. Selected interatomic bond distances (Å) are as follows: Au1−Os1 = 2.7541(5), Au1−Os2 = 2.7917(5), Os1−Os2 = 2.8799(5), Os1−Os3 = 3.0044(5), Os2−Os3 = 2.7525(5), Os1−C35 = 2.134(10), Os2−C35 = 2.300(9), Os2−C36 = 2.441(9), Os3−C36 = 2.100(9), Os1−H1 = 1.54(7), Os3−H1 = 1.91(7).

SUMMARY AND CONCLUSIONS

It has been shown in this work that the reagents $ArylAu(PPh_3)$ (Aryl = phenyl, 2-naphthyl, and 1-pyryl) react with **1** by the loss of the two NCMe ligands from **1** and the oxidation-addition of the Au−C bond to yield the first examples of unsaturated metal carbonyl cluster complexes, **2**, **3a**, **4**, and **5**, containing η^1-bridging phenyl, η^1-bridging naphthyl, and η^1-bridging pyryl ligands, respectively. The 2-naphthyl ligand in **3b** coordinates to the metal cluster in a η^2-bridging mode. The η^2-bridging naphthyl in **3b** serves as a three-electron donor; thus the metal atoms in this complex are electronically saturated. Two isomers, **4** and **5**, were obtained in the reaction of **1** with $1\text{-PyrylAu}(PPh_3)$. A DFT computational analysis has revealed that bonding of the bridging phenyl ligand to the metal atoms in **2** consists of a combination of delocalized σ-bonding between the ipso-carbon atom and the two proximate metal atoms and π-donation from the π-orbitals of the ring to those same metal atoms. There is no significant metal to ring π-back-bonding. It has been demonstrated that the bridging aryl ligands can be converted into triply bridging aryne ligands in good yields by thermal decarbonylation reactions via the activation of a neighboring CH bond on the aryl ring. Efforts to establish the nature of the transformation from **3b** to **7** by computational methods have provided a mechanism predicated on elimination of CO at the $Os(CO)_4$ group in the cluster

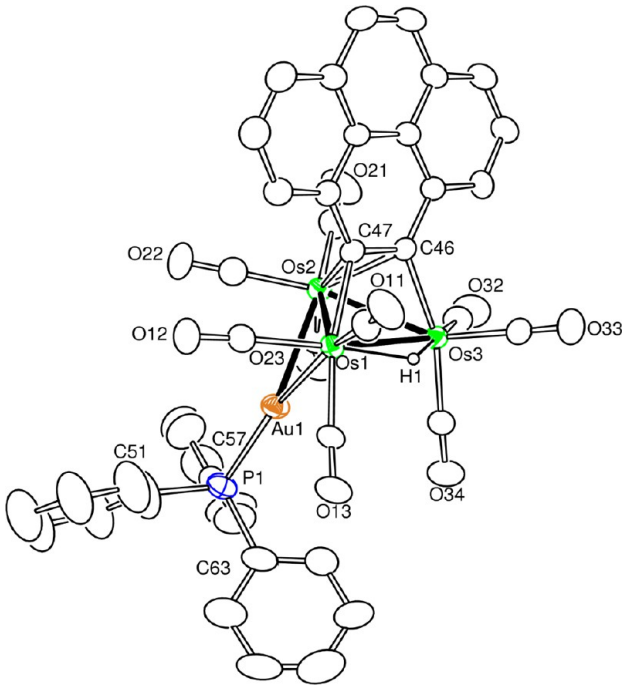

Figure 15. ORTEP diagram of the molecular structure of $Os_3(CO)_{10}(\mu_3$-4,5-pyryne$)(\mu$-AuPPh$_3)(\mu$-H), **9**, showing 30% thermal ellipsoid probability. The hydrogen atoms are omitted for clarity. Selected interatomic bond distances (Å) are as follows: Au1−Os1 = 2.7480(4), Au1−Os2 = 2.7909(4), Os1−Os2 = 2.8770(4), Os1−Os3 = 2.9702(4), Os1−C47= 2.144(7), Os2−Os3 = 2.7634(4), Os2−C46 = 2.303(7), Os2−C47 = 2.287(7), Os3−C46 = 2.115(7), Os1−H1 = 1.73(6), Os3−H1 = 1.78(6).

followed by CH bond cleavage at that metal atom. It is anticipated that other unsaturated polynuclear metal carbonyl cluster complexes containing bridging aryl ligands will be prepared in the future, and these may also exhibit interesting reactivity.

■ ASSOCIATED CONTENT

Supporting Information

Details of the computational analyses for **2** and the transformation of **3b** to **7**; experimental details for the structural analyses; and the CIF files for each of the structures **2**, **3a**, **3b**, **4**, **5**, **6**, **7**, **8**, and **9** are available. This material is available free of charge via the Internet at http://pubs.acs.org.

■ AUTHOR INFORMATION

Corresponding Author

*E-mail: Adamsrd@mailbox.sc.edu.

Notes

The authors declare no competing financial interest.

■ ACKNOWLEDGMENTS

This research was supported by the following grants from the National Science Foundation: CHE-1111496 and CHE-1048629.

■ REFERENCES

(1) Amatore, C.; Jutand, A. *Acc. Chem. Res.* **2000**, *33*, 314−321.
(2) Ackermann, L.; Vicente, R.; Kapdi, A. R. *Angew. Chem., Int. Ed.* **2009**, *48*, 9792−9826.
(3) Foley, N. A.; Lee, J. P.; Ke, Z.; Gunnoe, T. B.; Cundari, T. R. *Acc. Chem. Res.* **2009**, *42*, 585−597.
(4) (a) Van Koten, G. *J. Organomet. Chem.* **1990**, *400*, 283−301. (b) Stollenz, M.; Meyer, F. *Organometallics* **2012**, *31*, 7708−7727. (c) Meyer, E. M.; Gambarotta, S.; Floriani, C.; Chiesi-Villa, A.; Guastini, C. *Organometallics* **1989**, *8*, 1067−1079.
(5) (a) Bradford, C. W.; Nyholm, R. S.; Gainsford, G. J.; Guss, J. M.; Ireland, P. R.; Mason, R. *J. Chem. Soc., Chem. Commun.* **1972**, 87−89. (b) Arce, A. J.; Arrojo, P.; Deeming, A. J.; De Sanctis, Y. *J. Chem. Soc., Chem. Commun.* **1991**, 1491−1492. (c) Adams, R. D.; Captain, B.; Zhu, L. *Inorg. Chem.* **2007**, *46*, 4605−4611. (d) Deng, M.; Leong, W. K. *J. Chem. Soc., Dalton Trans.* **2002**, 1020−1023. (e) Adams, R. D.; Pearl, W. C., Jr. *J. Organomet. Chem.* **2011**, *696*, 1198−1210. (f) Garcia, M. E.; Ramos, A.; Ruiz, M. A.; Lanfranchi, M.; Marchio, L. *Organometallics* **2007**, *26*, 6197−6212. (g) Briard, P.; Cabeza, J. A.; Llamazares, A.; Ouahab, L.; Riera, V. *Organometallics* **1993**, *12*, 1006−1008. (h) Cabeza, J. A.; Franco, R. J.; Llamazares, A.; Riera, V. *Organometallics* **1994**, *13*, 55−59.
(6) (a) Moret, M.-E.; Chen, P. *Organometallics* **2008**, *27*, 4903−4916. (b) Moret, M.-E.; Chen, P. *J. Am. Chem. Soc.* **2009**, *131*, 5675−5690. (c) Fernandez, E. J.; Laguna, A.; Lopez-de-Luzuriaga, J. M.; Monge, M.; Montiel, M.; Elena Olmos, M.; Rodriguez-Castillo, M. *Organometallics* **2006**, *25*, 3639−3646.
(7) Adams, R. D.; Chen, M.; Zhang, Q. *Organometallics* **2013**, *32*, 2416−2426.
(8) (a) Adams, R. D.; Kan, Y.; Zhang, Q. *Organometallics* **2011**, *30*, 328−333. (b) Farrugia, L. J.; Miles, A. D.; Stone, F. G. A. *J. Chem. Soc., Dalton Trans.* **1984**, 2415−2422. (c) Hoferkamp, L. A.; Rheinwald, G.; Stoeckli-Evans, H.; Suss-Fink, G. *Organometallics* **1996**, *15*, 704−712. (d) Shima, T.; Suzuki, H. *Organometallics* **2005**, *24*, 1703−1708. (e) Akita, M.; Hua, R.; Oku, T.; Tanaka, M.; Moro-oka, Y. *Organometallics* **1996**, *15*, 4162−4177. (f) Alvarez, M. A.; Garcia, M. E.; Martinez, M. E.; Ramos, A.; Ruiz, M. A. *Organometallics* **2009**, *28*, 6293−6307.
(9) Goudsmit, R. J.; Johnson, B. F. G.; Lewis, J.; Raithby, P. R.; Rosales, M. J. *J. Chem. Soc., Dalton Trans.* **1983**, 2257−2261.
(10) Brait, S.; Deabate, S.; Knox, S. A. R.; Sappa, E. *J. Cluster Sci.* **2001**, *12*, 139−173.
(11) Johnson, B. F. G.; Nairn, J. G. M.; Brown, D. B.; Lewis, J.; Gallop, M.; Parker, D. G. *Chem.—Eur. J.* **1995**, *1*, 252−260.
(12) (a) Raubenheimer, H. G.; Schmidbaur, H. *Organometallics* **2012**, *31*, 2507−2522. (b) Stone, F. G. A. *Angew. Chem., Int. Ed. Engl.* **1984**, *23*, 89−99. (c) Evans, D. G.; Mingos, D. M. P. *J. Organomet. Chem.* **1982**, *232*, 171−191.
(13) Adams, R. D.; Chen, M. *Organometallics* **2012**, *31*, 6457−6465.
(14) Adams, R. D.; Rassolov, V.; Zhang, Q. *Organometallics* **2012**, *31*, 2961−2964.
(15) (a) Deeming, A. J. *Adv. Organomet. Chem.* **1986**, *26*, 1−96. (b) Keister, J. B.; Shapley, J. R. *J. Am. Chem. Soc.* **1976**, *98*, 1056−1057. (c) Hudson, R. H. E.; Poe, A. J. *Organometallics* **1995**, *14*, 3238−3248.
(16) Adams, R. D.; Rassolov, V.; Zhang, Q. *Organometallics* **2013**, *32*, 1587−1590.
(17) Braga, D.; Grepioni, F.; Parisini, E.; Johnson, B. F. G.; Martin, C. M.; Nairn, J. G. M.; Lewis, J.; Martinelli, M. *J. Chem. Soc., Dalton Trans.* **1993**, 1891−1895.
(18) PartyKa, D. V.; Zeller, M.; Hunter, A. D.; Gray, T. G. *Angew. Chem., Int. Ed.* **2006**, *45*, 8188−8191.
(19) Osawa, M.; Hoshino, M.; Hashizume, D. *Dalton Trans.* **2008**, 2248−2252.
(20) Heng, W. Y.; Hu, J.; Yip, J. H. K. *Organometallics* **2007**, *26*, 6760−6768.
(21) Hay, C. M.; Leadbeater, N. E.; Lewis, J.; Raithby, P. R.; Burgess, K. *New J. Chem.* **1998**, *22*, 787−788.
(22) *SAINT+*, version 6.2a; Bruker Analytical X-ray Systems, Inc.: Madison, WI, 2001.
(23) Sheldrick, G. M. *SHELXTL*, version 6.1; Bruker Analytical X-ray Systems, Inc.: Madison, WI, 1997.
(24) *ADF2012*, SCM, Theoretical Chemistry, Vrije Universiteit: Amsterdam, The Netherlands, http://www.scm.com.

(25) Perdew, J. P.; Ruzsinszky, A.; Csonka, G. I.; Vydrov, O. A.; Scuseria, G. E. *Phys. Rev. Lett.* **2008**, *100*, 136406.
(26) Arce, A. J.; Arrojo, P.; Deeming, A. J.; De Sanctis, Y. *J. Chem. Soc., Chem. Commun.* **1991**, 1491−1492.
(27) (a) Broach, R. W.; Williams, J. M. *Inorg. Chem.* **1979**, *18*, 314−319. (b) Churchill, M. R.; Hollander, F. J.; Hutchinson, J. P. *Inorg. Chem.* **1977**, *16*, 2697−2700. (c) Allen, V. F.; Mason, R.; Hitchcock, P. B. *J. Organomet. Chem.* **1977**, *140*, 297−307.
(28) Burgess, K.; Johnson, B. F. G.; Kaner, D. A.; Lewis, J.; Raithby, P. R.; Syed,-Mustaffa, S. N. A. B. *J. Chem. Soc., Chem. Commun.* **1983**, 455−457.
(29) Johnson, B. F. G.; Kaner, D. A.; Lewis, J.; Raithby, P. R. *J. Organomet. Chem.* **1981**, *215*, C33−C37.
(30) Cullen, W. R.; Rettig, S. J.; Zheng, T. C. *Organometallics* **1995**, *14*, 1466−1470.
(31) Connor, J. A. In *Transition Metal Clusters*; Johnson, B. F. G., Ed.; John Wiley & Sons: Chichester, 1980; Chapter 5, pp 345−363.
(32) Arce, A. J.; Canavera, F.; De Sanctis, Y.; Ascanio, J.; Machado, R.; Gonzalez, T. *J. Organomet. Chem.* **2009**, *694*, 1834−1839.